Research Square

Preprints are preliminary reports that have not undergone peer review.
They should not be considered conclusive, used to inform clinical practice,
or referenced by the media as validated information.

Carbon-Fixation Potential in Zhuqueibacterota from a Central Indian Ridge Hydrothermal Vent Extends beyond Zhuqueibacterales, Tracking Habitat Rather Than Lineage

Mi-Jeong Park
Korea Institute of Ocean Science & Technology
Yun Jae Kim
Korea Institute of Ocean Science & Technology
Joungmin Lee
Korea Institute of Ocean Science & Technology
Jihyun Yu
Korea Institute of Ocean Science & Technology
Gyeong-Hak Han
Korea Institute of Ocean Science & Technology
Jung-Hyun Lee
Korea Institute of Ocean Science & Technology
Kae Kyoung Kwon
kkkwon@kiost.ac.kr

Korea Institute of Ocean Science & Technology

Research Article

Keywords:

Posted Date: November 9th, 2026

DOI: https://doi.org/10.21203/rs.3.rs-10841408/v1

License: This work is licensed under a Creative Commons Attribution 4.0 International License.
Read Full License

Additional Declarations: No competing interests reported.

Carbon-Fixation Potential in *Zhuqueibacterota* from a Central Indian Ridge Hydrothermal Vent Extends beyond *Zhuqueibacterales*, Tracking Habitat Rather Than Lineage

Mi-Jeong Park[1], Yun Jae Kim[1,2], Joungmin Lee[1,2], Jihyun Yu[1,2], Gyeong-Hak Han[1,2], Jung-Hyun Lee[1,2] and Kae Kyoung Kwon[1,2*]

[1]Korea Institute of Ocean Science & Technology, Marine Biotechnology Research Center, Busan, Republic of Korea

[2]University of Science and Technology, Department of Applied Ocean Science, Daejeon, Republic of Korea

E-mail & ORCID: Mi-Jeong Park (mijeong16@kiost.ac.kr/0000-0002-4965-5476); Yun Jae Kim (bio1213@kiost.ac.kr/0000-0002-6069-7909); Joungmin Lee (leejm516@kiost.ac.kr/0000-0002-3722-3756); Jihyun Yu (jihyunyu@kiost.ac.kr/0009-0000-9065-8364); Gyeong Hak Han (asdf7341@kiost.ac.kr/0009-0003-3925-3371); Jung-Hyun Lee (jlee@kiost.ac.kr/0000-0003-0787-2592); Kae Kyoung Kwon (kkkwon@kiost.ac.kr/0000-0002-0606-4545)

***Corresponding authors:** Kae Kyoung Kwon (kkkwon@kiost.ac.kr)

Keywords: KSB1, Central Indian Ridge, hydrothermal vent, carbon fixation, shotgun metagenomics, *Zhuqueibacterota*, *Oceanimicrobiales*, *Geothermoviventales*, *Abyssisedimentimicrobiales*, JDFR-76

Abstract

Background

Deep-sea hydrothermal vent fields are biological hotspots sustained by chemosynthetic primary production rather than photosynthesis. The Onnuri Vent Field (OVF), discovered in 2018 on the Central Indian Ridge, exhibits an unusual diffuse-flow regime and supports a distinct faunal community, yet its microbial contributors to primary production remain incompletely characterized. *Zhuqueibacterota* (formerly Ca. KSB1) is an uncultured bacterial phylum long considered strictly heterotrophic, although a recent study proposed that a single order within this phylum, *Zhuqueibacterales*, can perform carbon fixation via the Calvin-Benson-Bassham (CBB) cycle. Because CBB-competent *Zhuqueibacterales* had not previously been reported from deep-sea hydrothermal vents, whether *Zhuqueibacterota* inhabiting the OVF belong to this order, and whether their capacity for carbon fixation extends to this environment, remained unexamined.

Results

Comparative shotgun metagenomic analysis of sediment from the OVF and two co-located chimney-type vent fields, Edmond and Solitaire, revealed a prokaryotic community at the OVF marked by the near-absence of *Epsilonproteobacteria*, the typically dominant chemolithoautotrophic primary producers at hydrothermal vents. Metagenome-assembled genome analysis identified *Zhuqueibacterota* as a lineage with high relative abundance unique to the OVF, encoding the complete gene set for carbon fixation via non-canonical CBB cycle variants. *Zhuqueibacterota*-derived RuBisCO sequences accounted for 7.2% of total RbcL sequences at the OVF, the second-largest contribution after *Gammaproteobacteria*. This carbon-fixing genome belonged to *Oceanimicrobiales* rather than *Zhuqueibacterales*, the order previously reported as the sole lineage capable of the CBB cycle. Phylogenetic analysis showed that possession of Form I RuBisCO, and thus the potential for active CBB cycle operation, tracked with isolation habitat rather than taxonomic lineage across the phylum, a pattern corroborated by global mapping of *Zhuqueibacterota*-derived RbcL sequences against environmental metagenomes.

Conclusions

The identification of a carbon-fixing *Zhuqueibacterota* genome within *Oceanimicrobiales*, rather than the previously implicated *Zhuqueibacterales*, demonstrates that CBB cycle capacity within this phylum cannot be inferred from order-level taxonomy alone. Instead, the association between Form I RuBisCO possession and isolation habitat, corroborated by global metagenomic mapping, indicates that habitat exerts a stronger influence on carbon-fixation potential than phylogenetic lineage in *Zhuqueibacterota*. These findings identify *Zhuqueibacterota* as an unrecognized contributor to carbon fixation in deep-sea hydrothermal vent ecosystems.

Background

In marine ecosystems, primary production is predominantly carried out by photosynthetic microalgae and phytoplankton in the photic zone [1, 2]. Because sufficient light energy for photosynthesis is generally available only to a depth of about 200m [3], deep-sea environments were historically assumed to depend entirely on organic matter sinking from the surface ocean as marine snow. However, the substantially higher organismal density at hydrothermal vent fields compared with

the surrounding deep seafloor demonstrates that these ecosystems cannot be sustained by marine snow alone [4]. The discovery of deep-sea hydrothermal vents in 1977 on the Galápagos Rift identified an ecosystem in which chemosynthesis, rather than photosynthesis, is the predominant form of organic carbon production [5, 6]. Hydrothermal vents are now recognized as chemosynthesis-based ecosystems (CBEs), in which primary productivity is fueled by chemical energy derived from vent fluids rather than light [7-10].

Seafloor massive sulfides that accumulate around hydrothermal vents contain high concentrations of copper, zinc, gold, and silver, and interest in their extraction has grown as terrestrial reserves of these metals decline [11]. Under the recommendations of the International Seabed Authority (ISA) for implementing the agreement under the United Nations convention on the law of the sea on the conservation and sustainable use of marine biological diversity of areas beyond national jurisdiction (BBNJ agreement), however, deep-sea exploration and mining are required to be accompanied by biodiversity research supporting the conservation and restoration of these ecosystems [12]. Microbial and macrofaunal biomass at hydrothermal vents are typically elevated relative to the surrounding deep sea owing to in situ primary production by chemolithotrophic bacteria, which form the base of the food web as free-living microbes, epibionts, or endosymbionts within macrofaunal hosts [13]. Because vent ecosystems depend on carbon fixation by these chemosynthetic primary producers, characterizing the bacteria responsible for primary production is essential to understanding the mechanisms that sustain hydrothermal vent ecosystems.

On slow-spreading ridges, low melt production favors the formation of deep faults and the tectonic exposure of mantle rocks at the seafloor, facilitating deep seawater penetration and hydrothermal fluid circulation, and thereby promoting hydrothermal vent formation [14]. The Central Indian Ridge (CIR) is a slow-to-intermediate spreading center with an expansion rate of 20 to 80 mm/yr [15], along which at least seven named active hydrothermal vent fields have been identified to date: Kairei, Edmond, Solitaire, Dodo, Onnuri, Onbada, and Onnarae [16-20]. Onnuri Vent Field (OVF), first discovered during a 2018 expedition targeting new hydrothermal vent fields on the CIR and formally reported in 2020, is located at approximately 2,000 m depth at the summit of an oceanic core complex (OCC-3-2), where it discharges ultramafic-hosted hydrothermal fluid. Chimney-type vents discharge high-temperature fluids through focused flow, whereas diffuse vents emit lower-temperature fluids (<100°C) through seafloor cracks, generating a mixing zone between reduced hydrothermal fluids and oxygenated seawater [21-23]. The OVF departs from this typical diffuse-flow profile: fluid temperatures exceeding 200°C have been recorded despite its diffuse venting style [24], together with strong oxidation-reduction potential (ORP) anomalies, high CH_4 concentrations, low metal concentrations, and evidence of both serpentinization and magmatic influence on fluid composition. These features indicate a hydrothermal regime more complex than that of typical diffuse-flow or chimney-type systems and suggest that the OVF may sustain a correspondingly distinct ecosystem, warranting biodiversity research.

The OVF hosts a diverse biological community, including holoplanktonic [25] and meroplanktonic larvae [26], bathymodiolin mussels (*Gigantidas vrijenhoeki* and *Bathymodiolus septemdierum*) [27-30], hairy snails (*Alviniconcha marisindica*) [31], shrimp (*Rimicaris kairei* and *Alvinocaris* sp.) [32], bythograeid crabs (*Austinograea rodriguezensis*) [33-35], squat lobsters (*Munidopsis lauensis*) [36], the parasitic scale worm *Branchipolynoe onnuriensis* [37, 38], harpacticoid copepods (*Smacigastes* sp. [39], *Barathricola thermophilus* [40]), the ciliate *Dysteria parasemilunaris* [41], the gastropod *Lophocochlias parvissimus* [42], and meiofauna dominated by nematodes (particularly *Chromadorita* and *Cobbia*) [20, 43], with a community structure that differed markedly from that of the surrounding deep sea. Notably, *G.*

vrijenhoeki and its parasitic polychaete *B. onnuriensis* were found exclusively at the OVF among Indian Ocean vent fields [37]. Based on 16 recovered taxa, seven trophic guilds and four trophic levels have been recognized within the OVF food web [44], indicating a food web structure of comparable complexity to that reported at other chemosynthesis-based ecosystems. The OVF has been the subject of extensive geological, geochemical, and faunal investigation, whereas microbiological characterization of its ecosystem has remained comparatively limited.

Previous microbiological studies of the OVF have provided preliminary insights into its microbial community structure and metabolic potential, largely through community-level profiling and symbiont-focused analyses. Amplicon and shotgun metagenomic analyses revealed that *Gammaproteobacteria* dominate the OVF microbial community, with predicted functional enrichment in sulfur cycling and single-carbon compound degradation, including methylotrophy and methanotrophy [45]. Functional gene surveys further demonstrated that CBB cycle genes (*rbcLS*) were more abundant at the OVF than at the adjacent Invent E vent field, with sequences most closely affiliated with the Gammaproteobacterial genera *Nitrosococcus* and *Allochromatium*, while rTCA cycle-related genes were more prevalent at Invent E [46]. Stable isotope analyses of OVF macrofauna identified at least three potential chemosynthetic carbon fixation routes: the CBB cycle, the reductive tricarboxylic acid (rTCA) cycle, and methanotrophic production [44]. Detection of a single marker gene, however, does not confirm that a complete carbon-fixation pathway is encoded; genome-resolved metagenomic analysis is therefore needed to identify previously unrecognized primary producers at the OVF that encode the complete gene set required for a functional pathway.

One such candidate is *Zhuqueibacterota* (formerly candidate division KSB1), an uncultured bacterial lineage first detected in 2000 as a 16S rRNA gene fragment in sulfur-rich coastal sediment [47]. Members of this phylum have since been reported as dominant taxa in freshwater and seawater bioreactors, caves, and deep-sea hydrothermal vents, yet their ecological role in each of these habitats remains poorly resolved. Because *Zhuqueibacterota* remains uncultured, inferences about its function have relied entirely on genomic data. Genomic surveys have predicted capabilities for carbohydrate hydrolysis, β-oxidation, anaerobic degradation of aromatic hydrocarbons, and alcohol fermentation, leading to the presumption that *Zhuqueibacterota* functions as an obligate chemoheterotroph [48-51]. Lian *et al.* renamed *Ca.* KSB1 as *Zhuqueibacterota* and, based on comparative MAG analysis, proposed that the phylum comprises five orders rather than the six recognized under GTDB-based taxonomy. Notably, MAGs affiliated with the order *Zhuqueibacterales* were predicted to perform autotrophic carbon fixation via the CBB cycle [52].

In this study, we performed genome-resolved shotgun metagenomic comparative analysis across three CIR vent fields, the diffuse-flow OVF and the focused high-temperature chimney vents Edmond and Solitaire, to identify previously unrecognized primary producers contributing to carbon fixation at the OVF. We further assessed whether such carbon-fixation potential, exemplified by the recently reported CBB-cycle activity in certain *Zhuqueibacterota* orders recovered from hot springs, extends to *Zhuqueibacterota* populations inhabiting deep-sea hydrothermal vents, and whether this capacity is restricted to a specific taxonomic order within the phylum.

Methods

Sampling Locations and Collection Procedures

A deep-sea research expedition was conducted aboard the R/V *Onnuri* by the Korea Institute of Ocean Science

and Technology (KIOST) from June 9 to July 4, 2018, to investigate hydrothermal vent ecosystems along the Central Indian Ridge (CIR). Sampling targeted three active vent fields: Edmond (23°52.69'S, 69°35.83'E; [25]), Solitaire (19°33.413'S, 65°50.888'E; [18]), and the newly identified Onnuri vent field (11°24.9'S, 66°25.4'E), which was first documented during this cruise [19]. Sediment and chimney materials were collected using a remotely operated Video-guided hydraulic grab sampler (TV-Grab, designated as GTV; OKTOPUS GmbH, Germany). The GTV was deployed at locations corresponding to the vent plume and seafloor contact sites. Immediately following recovery, samples designated for metagenomic analysis were subsampled under sterile conditions and stored onboard at -80 °C. Detailed sampling coordinates and associated metadata for all collections are provided in Supplementary Table 1, and the site maps are presented in Supplementary Fig. 1.

DNA Extraction and High-Throughput Sequencing

DNA extraction was performed using the FastDNA SPIN Kit for Soil (MP Biomedicals, Irvine, CA, USA) following the manufacturer's protocol. For each sediment sample originating from the three vent-field locations, 500 mg of wet sediment was transferred into four separate extraction tubes, resulting in a total wet weight of 2 g per sample location. The lysis step involved bead-beating for 30 min at maximum speed using a Vortex Genie. Following purification and isopropanol precipitation, the resulting DNA pellet was resuspended in 300 µL of 10 mM Tris buffer (pH 8.0). DNA concentration and purity were assessed using a Qubit fluorometer (Thermo Fisher) and a NanoDrop spectrophotometer (Thermo Fisher), respectively. Shotgun metagenomic library preparation and sequencing were performed on an Illumina MiSeq platform using the v3 reagent kit (2 x 300 bp paired-end) at the LAS sequencing facility (Gimpo, Republic of Korea). All procedures were carried out in a clean laboratory environment, and negative extraction controls (no sediment input) were processed in parallel with the samples during DNA extraction to monitor for potential contamination. The extraction controls yielded no detectable DNA and consequently did not meet the minimum input requirement for library preparation.

Raw Data Processing and Assembly

Raw paired-end reads were subjected to quality control filtering using Skewer v0.2.2 [53]. The filtering criteria included a minimum base quality threshold of Q30, a minimum read length of 200 bp (–l 200), and automatic adapter detection (–f auto). PhiX174 spike-in sequences were subsequently removed using BBTools v37.62 (hdist = 1, k = 31) [54]. Following preprocessing, the Edmond, Solitaire, and Onnuri samples yielded 9,226,772, 10,325,276, and 12,420,385 high-quality read pairs, respectively, corresponding to a read retention rate of 85.45 ± 2.23 % across all samples. After merging the filtered read sets, a total of 17,949,744 ± 2,326,681 reads were retained for downstream analyses (Supplementary Table 2). Filtered reads were assembled using MetaSPAdes v3.13.0 with iterative k-mer sizes of 21, 33, 55, 77, and 99 [55]. To enhance the quality of subsequent metagenomic binning and annotation, contigs shorter than 1 kb were removed from the assembly output. Taxonomic assignment of contigs was performed using two complementary strategies: (i) k-mer–based classification with Kraken2 v2.1.6 [56] followed by abundance re-estimation with Bracken v3.0.1 [57], and (ii) protein-level six-frame translation–based classification using Kaiju v1.10.1 [58]. Kraken2–Bracken provided high-resolution taxonomic profiling optimized for nucleotide-level assignments, whereas Kaiju enabled the classification of highly divergent sequences and genomes lacking close

reference representatives. The combined use of these methods was intended to improve taxonomic accuracy for deep-sea hydrothermal microbial communities, which are known to contain a high proportion of uncharacterized lineages.

Carbon Fixation Pathway Abundance Analysis

Open reading frames (ORFs) were predicted from the assembled contigs using Prodigal v2.6.3 [59] with the '–p meta' option. The resulting protein sequences (FAA files) were subsequently annotated using EggNOG-mapper v2.1.12 [60] against the eggNOG database v5.0.2 [61]. Key enzymes involved in the seven major carbon fixation pathways—the reductive tricarboxylic acid (rTCA) cycle, Calvin-Benson-Bassham (CBB) cycle, 3-hydroxypropionate (3-HP) cycle, Wood-Ljungdahl (WL) pathway, dicarboxylate–4-hydroxybutyrate (DC/4HB) cycle, 3-hydroxypropionate–4-hydroxybutyrate (3HP/4HB) cycle, and reductive glycine (rGly) pathway—were identified based on KEGG Orthology (KO) numbers. The complete list of KO identifiers used for pathway reconstruction is detailed in Supplementary Table 3. To quantify pathway abundance, quality-filtered paired-end reads were mapped back to the ORF nucleotide sequences using BWA-MEM v0.7.18 [62], and alignment files were processed with SAMtools v1.21 [63]. Gene-level abundance was estimated as Transcripts Per Million (TPM) [64], calculated by normalizing read counts by gene length (reads per kilobase, RPK) followed by library size normalization. TPM values were subsequently aggregated across all enzymes assigned to each pathway to derive pathway-level abundances, which were then compared among the Edmond, Solitaire, and Onnuri vent fields.

Metagenome Assembled Genomes (MAGs) Binning

For binning with CONCOCT, assembled contigs were split into 10-kb fragments to minimize assembly artifacts and reduce length bias during clustering; contigs shorter than 20 kb were not fragmented. Genome binning was performed using three independent algorithms: CONCOCT v1.1.0 [65], MetaBAT2 v2.18 [66], and MaxBin2 v2.2.7 [67], yielding 245, 139, and 364 preliminary bins, respectively. The resulting bin sets were integrated and dereplicated using DAS Tool v1.1.7 [68], producing 66 non-redundant MAGs. These MAGs were further refined with RefineM v0.1.2 [69], which employs DIAMOND-based taxonomic profiling to remove contigs with inconsistent phylogenetic signals. The quality of the refined MAGs was assessed using CheckM v1.2.3 [70]. According to the Minimum Information about a Metagenome-Assembled Genome (MIMAG) standards [71], MAGs with completeness >90% and contamination <5% were classified as high-quality MAGs (HQ-MAGs), whereas those with completeness ≥50% and contamination <10% were classified as medium-quality MAGs (MQ-MAGs). Only 45 MAGs of medium quality or higher were retained for downstream analyses. Taxonomic assignment of these MAGs was performed using the *classify_wf* module of GTDB-Tk v1.7.0 [72].

MAGs Abundance, Replication Activity, and Functional Annotation

To compare the relative abundance of MAGs across sampling sites, quality-filtered reads were mapped back to the reconstructed MAGs, and MAG-level abundance values were calculated based on mapped read counts. Abundances were normalized using TPM to account for differences in sequencing depth among samples. Replication activity of individual MAGs was estimated using GRiD (Growth Rate index) v1.3 [73]. GRiD infers in situ

replication rates based on coverage gradients along the genome, specifically considering coverage ratios between the origin of replication (*dnaA*/*ori*) and the terminus region (*ter*/*dif*). Functional annotation of MAGs was performed using DRAM v1.5.0 [74] with the annotate and distill modules, applying a minimum contig size threshold of 500 bp. Annotations were generated based on multiple reference databases, including KOfam [75], UniRef90 [76], Pfam [77], dbCAN [78], and VOGDB [79]. To assess the taxonomic origin of RuBisCO genes, protein sequences were identified by filtering annotations corresponding to KEGG orthology K01601, and taxonomic information associated with these annotations was extracted. The relative contribution of each taxon was calculated as the proportion of RuBisCO annotations assigned to that taxon.

Collection, Dereplication, and Phylogenomic Analysis of *Zhuqueibacterota* MAGs

To construct a comprehensive reference dataset of *Zhuqueibacterota*-related genomes, publicly available MAGs were collected from multiple sources as of October 2024, including 146 genomes from NCBI, 99 genomes from GTDB, 53 genomes from the GEMs catalog (A Genomic Catalog of Earth's Microbiomes, JGI), and 11 genomes reported in previously published studies. Genomes were filtered based on quality metrics, retaining only MAGs with estimated completeness >70%, contamination <10%, and a quality score (QS) ≥55. Taxonomic affiliation to the *Zhuqueibacterota* lineage was verified using GTDB-Tk, and only genomes consistently classified as *Zhuqueibacterota* (*Ca.* KSB1) were included. Dereplication of the collected genomes together with *Zhuqueibacterota* MAGs recovered in this study was performed using dRep v3.6.2 [80], with parameters -sa 0.99 and -nc 0.50 to remove highly similar genomes at near-strain resolution, yielding a final non-redundant dataset of 100 *Zhuqueibacterota* MAGs (Supplementary Table 4). Phylogenomic relationships among the dereplicated genomes were reconstructed using the bacterial 120 single-copy core gene set (bac120) identified by GTDB-Tk. Individual marker genes were aligned using MAFFT v7.526 [81], and partitioned concatenated alignments were generated. Maximum-likelihood phylogenetic trees were inferred with IQ-TREE v2.4.0 [82] using the Model Finder Plus (MFP) option with 1,000 ultrafast bootstrap replicates (-bb 1000 -alrt 1000). To further validate tree topology, an independent phylogenetic tree was reconstructed using PhyloPhlAn3 with 400 amino acid markers, and bootstrap support values obtained from both IQ-TREE (ultrafast bootstrap and SH-aLRT) and PhyloPhlAn3 were used to assess the robustness of the inferred topology. As outgroups, type species representing major lineages within the FCB superphylum – including *Bacteroidota*, *Chlorobiota*, *Fibrobacterota*, *Fidelibacteria*, and *Gemmatimonadota* – were selected to root the tree. To further evaluate genomic relatedness among *Zhuqueibacterota* MAGs and confirm phylum-level coherence, pairwise average amino acid identity (AAI) values were calculated using EzAAI v1.2.3 [83]. Effect sizes for these pairwise comparisons were calculated as Cliff's delta using the *effsize* package v0.8.1 in R, with magnitudes classified as negligible ($|\delta|<0.147$), small ($0.147\leq|\delta|<0.33$), medium ($0.33\leq|\delta|<0.474$), or large ($|\delta|\geq0.474$) according to established thresholds [84].

Detection of CBB Cycle Enzymes, Phylogenetic Analysis of RbcL, and Global Mapping

KEGG Orthology (KO) annotations for the *Zhuqueibacterota* MAG dataset were obtained using GhostKOALA [85]. Environmental source information for RbcL-containing *Zhuqueibacterota* MAGs was assigned based on metadata associated with each genome. The presence or absence of genes corresponding to both canonical and non-

canonical Calvin-Benson-Bassham (CBB) cycle pathways was determined according to KO identifiers. For phylogenetic analysis of, RbcL sequences identified from *Zhuqueibacterota* MAGs were analyzed together with reference sequences representing known RbcL forms (Supplementary Table 5). Multiple sequence alignment was performed using MAFFT, and poorly aligned or gap-rich regions were trimmed with trimAl v1.5 [86] using the -gt 0.05 option. A maximum-likelihood phylogenetic tree was reconstructed using IQ-TREE with the LG+R5 substitution model and branch support assessed with 1,000 ultrafast bootstrap replicates (-bb 1000 -alrt 1000). To investigate the global distribution of *Zhuqueibacterota*-associated RbcL genes, metagenomic sequences annotated as K01601 were retrieved from the Integrated Microbial Genomes & Microbiomes (IMG/M) database [87], yielding a total of 3,295,882 sequences. The maximum pairwise sequence identity among RbcL genes within the *Zhuqueibacterota* MAG dataset was 99.59%. To ensure conservative assignment, a stricter threshold of 99.6%, exceeding this intra-dataset maximum, was applied to global database hits. Global mapping was performed using DIAMOND BLASTp [88] with an e-value cutoff of 1e-5, and hits meeting these criteria were used to infer the environmental distribution of *Zhuqueibacterota*-derived RbcL sequences.

Results

Microbial community composition across three hydrothermal vent fields in the CIR

Microbial community composition across the three hydrothermal vent fields was assessed using Kraken2-Bracken and Kaiju classifiers; the two methods yielded highly consistent patterns at the phylum level (Fig. 1A). Notably, the OVF exhibited a substantially higher relative abundance of *Gammaproteobacteria* and a lower relative abundance of *Flavobacteria* compared with the Edmond and Solitaire vent fields, while *Epsilonproteobacteria* were present at extremely low relative abundances in the OVF. These compositional differences were also evident at the genus level (Fig. 1B). The sulfur-oxidizing genera *Sulfurovum* and *Sulfurimonas*, which were abundant in the Edmond and Solitaire vent fields, were detected at only very low levels in the OVF. Members of these genera are key chemolithoautotrophic microorganisms involved in carbon fixation and sulfur cycling in hydrothermal vent ecosystems. Another genus exhibiting clear site-specific enrichment was *Lutibacter*, which was abundant in the Edmond and Solitaire vent fields but relatively scarce in OVF. Genomic analysis of *Lutibacter profundi* LP1^{T}, isolated from chimney surface biofilms in Arctic deep-sea hydrothermal vents, revealed microaerophilic and organotrophic metabolic traits, with a complete denitrification pathway and genes involved in sulfide oxidation, indicating the capacity for energy acquisition through sulfide oxidation under oxygen-limited conditions [89]. Members of this genus have also been proposed as important degraders of organic matter, including nucleic acids, in sulfide-rich deep-sea environments [90, 91]. In contrast, the archaeal genus *Nitrosopumilus* was markedly enriched in the OVF. *Nitrosopumilus* species belong to ammonia-oxidizing archaea (AOA), which perform autotrophic ammonia oxidation via the sequential action of ammonia monooxygenase and hydroxylamine dehydrogenase [92-94]. Owing to their exceptionally high affinity for ammonia, AOA sustain growth even at the extremely low ammonia concentrations typical of oligotrophic deep-ocean environments [95], and are therefore considered important regulators of nitrogen cycling in the deep ocean. In addition, many AOA fix carbon via the 3HP/4HB cycle [96], contributing to chemosynthetic primary production in deep-sea ecosystems. Together, the

depletion of rTCA-associated *Epsilonproteobacteria* and the enrichment of *Gammaproteobacteria* and AOA at the OVF suggest a shift away from the canonical *Epsilonproteobacteria*-dominated, sulfur-based primary production typical of hydrothermal vents, toward alternative energy-acquisition and carbon-fixation strategies.

Carbon fixation potential across three hydrothermal vent fields in the Central Indian Ridge

To investigate whether differences in microbial community composition were associated with variations in carbon fixation potential across the three hydrothermal vent fields, the abundance of enzymes involved in seven known carbon fixation pathways–rTCA, CBB, 3-HP, WL, DC/4HB, 3HP/4HB, and rGly–was compared (Fig. 1C; Supplementary Table 6). Enzymes associated with the rTCA cycle were widely detected across all three sites; however, the key citrate-cleavage reactions showed markedly lower abundance in the OVF. Both known citrate-cleavage strategies–ATP citrate lyase (ACL) and the two-step system comprising citryl-CoA synthetase (*ccsA*) and citryl-CoA lyase (*ccl*)–were less prevalent in Onnuri than in the Edmond and Solitaire vent fields, consistent with the relatively low abundance of *Sulfurovum* and *Sulfurimonas*, whose members use the rTCA cycle as a primary carbon fixation pathway [97-99]. Genes encoding enzymes of the WL pathway were detected across all three vent fields, and the relatively uniform distribution of the Rnf complex suggests comparable energy conservation capacities linked to this pathway among sites [100]. However, enzymes involved in CO_2 and formate utilization–including carbon monoxide dehydrogenase (CODH) and formate dehydrogenase–were relatively enriched in the OVF, whereas formate-tetrahydrofolate ligase was more abundant in the Solitaire vent field, indicating site-specific variation in substrate utilization strategies within the WL pathway. The CBB cycle appeared broadly distributed across all three vent fields; however, key enzymes of the canonical CBB cycle, including fructose-1,6-/sedoheptulose-1,7-bisphosphatase (F/SBPase) and phosphoribulokinase (PRK), were less abundant in the OVF. This pattern suggests that carbon fixation at the OVF may proceed via a non-canonical, PPi-PFK-dependent variant of the CBB cycle [101].

MAG-based reconstruction reveals non-canonical CBB cycle potential in the OVF

Because pathway-level gene abundance alone cannot identify which taxa are responsible for this potential, metagenome binning was performed to reconstruct MAGs and identify previously unrecognized microbial contributors to primary production in the OVF. In total, 45 MAGs were recovered, comprising three archaeal and 42 bacterial genomes (Fig. 1D). Analysis of sample-specific relative abundance ($\log_{10}$TPM) and replication rates estimated using GRiD revealed that MAGs with high relative abundance at each site also tended to display elevated replication rates, indicating active microbial growth within their respective environments (Fig. 1E). Several MAGs displayed consistently high abundance and replication activity exclusively in the OVF, including IO2018_MAG_02 (*Nanoarchaeota*; *Pacearchaeales*), IO2018_MAG_03 (*Thermoplasmatota*; RBG-16-68-12), IO2018_MAG_04 (*Actinobacteriota*; UBA5794), IO2018_MAG_22-24 (KSB1; CR04bin15), IO2018_MAG_27-28 (*Planctomycetota*; *Pirellulales*), IO2018_MAG_29 (*Alphaproteobacteria*; Bin95), IO2018_MAG_31 (*Alphaproteobacteria*; *Rhodospirillales*), IO2018_MAG_32 (*Alphaproteobacteria*; *Sphingomonadales*), IO2018_MAG_33-34 (*Alphaproteobacteria*; *Acidiferrobacterales*), and IO2018_MAG_35 (*Alphaproteobacteria*; AKS1) (Supplementary Table 7). To assess their carbon fixation potential, gene content analysis was restricted to MAGs meeting

conservative quality thresholds (completeness ≥70%, contamination ≤5%, quality score ≥55) (Fig. 2A). Among the 11 MAGs enriched in the OVF, only IO2018_MAG_22 harbored a nearly complete gene set associated with carbon fixation via the CBB cycle. IO2018_MAG_22 lacks fructose-1,6-bisphosphatase class II/sedoheptulose-1,7-bisphosphatase (F/SBPase), indicating that the canonical CBB cycle is unlikely to operate in this lineage. However, this genome encodes ATP-dependent 6-phosphofructokinase (PPi-PFK) and transaldolase (TAL), indicating the potential operation of alternative CBB variants, including the PPi-PFK-dependent CBB cycle and the transaldolase-variant SBPase-less CBB cycle (Fig. 2B). The co-occurrence of PPi-PFK and transaldolase indicates the genomic potential to operate two alternative CBB variants rather than a single redundant pathway. The PPi-PFK-dependent CBB cycle requires less ATP than the canonical pathway, whereas the transaldolase-variant SBPase-less CBB cycle involves fewer enzymatic steps; both may represent energetically favorable strategies under energy-limited conditions. This co-occurrence may allow the lineage to adjust its carbon-fixation strategy according to energy availability in the hydrothermal vent environment [101].

We therefore focused subsequent analyses on IO2018_MAG_22. To identify the taxonomic origin of RuBisCO genes detected at the OVF, taxonomic classification of RuBisCO sequences was performed (Fig. 2C). Ca. KSB1 (*Zhuqueibacterota*) accounted for the second-largest contribution to RuBisCO sequences (7.2%) after *Gammaproteobacteria* (71%), a notable finding given that no prior study has reported carbon fixation by KSB1 in hydrothermal vent environments. A recent study demonstrated that certain lineages within KSB1, specifically *Zhuqueibacterales*, possess the capacity for carbon fixation via the CBB cycle in hot spring environments, leading to the proposal of a new phylum designation, *Zhuqueibacterota* [52]. Whether this autotrophic capacity extends to *Zhuqueibacterota* populations inhabiting hydrothermal vents, and whether this lineage functions as a genuine primary producer in such environments, has not been examined. We therefore characterized the taxonomic and genomic diversity of *Zhuqueibacterota* in greater detail.

Genome-based analyses redefine order-level diversity and carbon fixation potential of *Zhuqueibacterota*

According to Lian et al. [52], *Zhuqueibacterota* comprises a single class encompassing five orders–*Residuimicrobiales*, *Oleimicrobiales*, *Thermofontimicrobiales*, *Oceanimicrobiales*, and *Zhuqueibacterales*. However, genome-based phylogenetic analysis conducted in the present study revealed that *Zhuqueibacterota* comprises seven orders rather than five (Fig. 3A). This discrepancy arises from two observations. First, *Oleimicrobiales* was resolved as two independent clades, with one clade retaining the original designation (*Oleimicrobiales*) and the other representing a distinct, previously unrecognized lineage (Clade 4). Second, JDFR-76, which was classified as a sister phylum to *Zhuqueibacterota* by Lian et al. [52] but had previously been considered a subordinate order within KSB1 under GTDB-Tk classification, was placed within *Zhuqueibacterota* in our phylogenetic tree (Clade 7). To validate the placement of JDFR-76 within *Zhuqueibacterota*, average amino acid identity (AAI) analysis was performed (Fig. 3B, Supplementary Table 8). AAI values between JDFR-76 members and other *Zhuqueibacterota* members (JDFR-76 group) showed extensive overlap with those among *Zhuqueibacterota* members alone (internal group; Cliff's $\delta = -0.17$, small), whereas AAI values between the outgroup and either the JDFR-76 group or the internal group formed clearly separated distributions (Cliff's $\delta = 1.00$ for both comparisons, large). Based on phylogenetic topology and AAI analysis, we propose Clade 4 and Clade 7 as two

novel orders within the phylum *Zhuqueibacterota*, for which we propose the names *Geothermoviventales* ord. nov. and *Abyssisedimentimicrobiales* ord. nov., respectively. Among all *Zhuqueibacterota* MAGs examined, 26 were found to encode RuBisCO (Fig. 3A; colored backgrounds on MAG labels indicate isolation source; Supplementary Table 4). To further assess their carbon fixation potential, the presence of CBB cycle-associated enzymes was examined across these 26 MAGs (Fig. 3C). In contrast to previous findings, which suggested that only MAGs belonging to *Zhuqueibacterales* possessed the potential for carbon fixation via the CBB cycle [52], our results reveal a more complex distribution. Four of the 26 RuBisCO-encoding MAGs lacked GAPDH, PRK, and RPE, rendering RuBP regeneration impossible and thus precluding complete CBB cycle operation; three of these belonged to *Zhuqueibacterales*–073.GCA_011375275.1 (Lau Basin hydrothermal vent rock), 091.GCA_022072515.1 (alternating anaerobic and microaerobic bioreactor), and 093.GCA_034505955.1 (hot spring sediment)–and one belonged to *Residuimicrobiales*–010.3300025882.5 (anaerobic digestor sludge). Furthermore, two deep-sea-derived MAGs within *Oceanimicrobiales*–062.GCA_022574215.1 (Mariana Trench surficial sediment) and 068.IO2018_MAG_22 (Onnuri hydrothermal vent field sediment)–encoded a gene set consistent with complete CBB cycle operation, showing that the capacity for CBB-based carbon fixation within *Zhuqueibacterota* extends beyond *Zhuqueibacterales*.

RuBisCO sequence analysis of *Zhuqueibacterota* MAGs

Phylogenetic analysis of RuBisCO amino acid sequences derived from *Zhuqueibacterota* MAGs, together with reference sequences representing each RuBisCO form, revealed that the distribution of RuBisCO forms was not confined to specific orders but was instead associated with the isolation habitat of each MAG (Fig. 4A; Supplementary Table 4). MAGs derived from deep-sea habitats (hydrothermal vents and trenches) and terrestrial hot springs harbored Form I RuBisCO as the predominant form, along with additional copies of Form III and Form IV. In contrast, MAGs derived from bioreactors and cave wall deposits harbored Form III as the predominant form, along with Form II and Form IV, for which catalytic activity in the CBB cycle remains uncertain. Notably, while certain *Zhuqueibacterales* MAGs from bioreactor environments lacked Form I RuBisCO, IO2018_MAG_22, belonging to *Oceanimicrobiales* and recovered from the OVF, harbored Form I RuBisCO, further supporting its potential for active CBB cycle operation. To examine the global distribution of *Zhuqueibacterota*-derived RbcL sequences, metagenomic contig-level data from the IMG/M database were searched using DIAMOND BLASTp (Fig. 4B; Supplementary Table 9). Consistent with the patterns observed in Fig. 4A, Form I and Form III RuBisCO were predominant in metagenomes from hot springs, freshwater, and hydrothermal vent environments, whereas Form III was the dominant form in metagenomes from intertidal zones, cave biofilms, and activated sludge, followed by Form IV (Fig. 4C). Together, these findings indicate that habitat, rather than phylogenetic affiliation, is a primary determinant of RuBisCO form distribution within *Zhuqueibacterota*.

Discussion

The proposal by Lian et al. [52] that CBB cycle capacity within *Zhuqueibacterota* is confined to the order *Zhuqueibacterales* rests on a taxonomic framework of five orders. The present phylogenomic analysis revises this

framework to seven orders, a discrepancy driven by the resolution of *Oleimicrobiales* into two independent clades, one retaining the original designation and the other described here as *Geothermoviventales* ord. nov., and by the reassignment of JDFR-76, previously treated as a sister phylum, to a position within *Zhuqueibacterota* as *Abyssisedimentimicrobiales* ord. nov. This revised topology matters directly for the CBB cycle argument: once *Abyssisedimentimicrobiales* and *Geothermoviventales* are accounted for as internal lineages rather than external or unresolved groups, the taxonomic boundaries against which CBB-capable MAGs were mapped shift, and the carbon-fixing genome recovered from the OVF resolves unambiguously to *Oceanimicrobiales* rather than to *Zhuqueibacterales*. A single-order model of CBB capacity cannot accommodate this placement without treating *Oceanimicrobiales* as an independent origin of the pathway, which in turn implies that the trait cannot be diagnosed from order membership alone.

The habitat-tracking pattern observed here provides an alternative model that better accounts for the data than a lineage-restricted one. Among the 26 RuBisCO-encoding *Zhuqueibacterota* MAGs, CBB-cycle completeness did not partition by order: three *Zhuqueibacterales* MAGs (from a hydrothermal vent rock, a bioreactor, and hot spring sediment) and one *Residuimicrobiales* MAG (from anaerobic digestor sludge) lacked the genes required for RuBP regeneration, while two *Oceanimicrobiales* MAGs, one from the Mariana Trench and one from the OVF, retained a complete gene set. What distinguished the complete from the incomplete genomes was not order but isolation source, a pattern that recurred at the RuBisCO-form level: Form I, the form associated with active CBB operation, predominated in MAGs and in global IMG/M metagenomes from deep-sea and hot-spring habitats regardless of order, whereas Form III predominated in bioreactor- and cave-derived sequences, including in *Zhuqueibacterales* MAGs that would be predicted to retain Form I under a strictly lineage-based model. This convergence between the MAG-level and the global metagenome-level analyses indicates that the association with habitat is unlikely to reflect sampling artifacts specific to the *Zhuqueibacterota* MAG dataset, and instead points to habitat as the variable that more consistently predicts carbon-fixation potential across this phylum than taxonomic order.

Several limitations should be considered when interpreting these findings. First, gene content analysis was restricted to MAGs meeting a completeness threshold of ≥70%, which falls short of the high-quality standard (>90% completeness) recommended by MIMAG guidelines [71]; incomplete genome recovery may have led to underestimation of carbon fixation potential in MAGs where relevant genes were present but not assembled or binned, and the absence of a gene in an incomplete MAG cannot be interpreted with certainty as a true absence in the source organism. Second, sampling was restricted to a single expedition along one section of the Central Indian Ridge, with sediment collected once from each of the three vent fields without biological replication; the extent to which the community and functional patterns observed at the OVF generalize across other diffuse-flow vent systems, or vary temporally within the OVF itself, remains untested. Third, because *Zhuqueibacterota* remains uncultured, all inferences regarding its carbon-fixation capacity are based on genomic potential rather than direct physiological or biochemical evidence; the presence of a complete CBB cycle gene set does not confirm that the pathway is transcribed, translated, or active in situ, and future work using metatranscriptomic or stable-isotope-labeling approaches would be needed to validate functional carbon fixation by this lineage. Fourth, the global distribution analysis of *Zhuqueibacterota*-derived RbcL sequences relied on metagenomic assemblies deposited in the IMG/M database, which reflects the sampling and sequencing effort of the broader research community rather than a systematic

environmental survey; habitats that are more heavily represented in public repositories may therefore appear disproportionately enriched for *Zhuqueibacterota*-derived RuBisCO, and the true environmental distribution of this lineage's carbon-fixation potential may extend to habitats currently underrepresented in available metagenomic data.

Conclusion

Genome-resolved metagenomic analysis of the Onnuri vent field identified *Zhuqueibacterota* as a previously unrecognized contributor to carbon fixation at a deep-sea hydrothermal vent, a habitat in which this capacity had not been reported. Contrary to the proposal that CBB cycle activity within *Zhuqueibacterota* is restricted to the order *Zhuqueibacterales*, the CBB-competent MAG recovered from the OVF belonged to *Oceanimicrobiales*, and genome-based and RuBisCO phylogenetic analyses indicated that RuBisCO form distribution across the phylum tracks with isolation habitat rather than taxonomic lineage. Global mapping of *Zhuqueibacterota*-derived RbcL sequences against environmental metagenomes further supported this habitat-driven pattern: Form I RuBisCO, the form associated with active CBB cycle operation, was specifically enriched in metagenomes from hydrothermal vents, terrestrial hot springs, soil, and freshwater, whereas metagenomes from bioreactor-associated habitats predominantly harbored Form III RuBisCO and Form IV RuBisCO-like proteins, whose contribution to the CBB cycle remains uncertain or absent. Together, these findings support recent evidence that *Zhuqueibacterota*, despite remaining uncultured and functionally uncharacterized across most of its habitats, can act as a CBB-based primary producer, and indicate that this role is contingent on habitat rather than a fixed, phylum-wide trait.

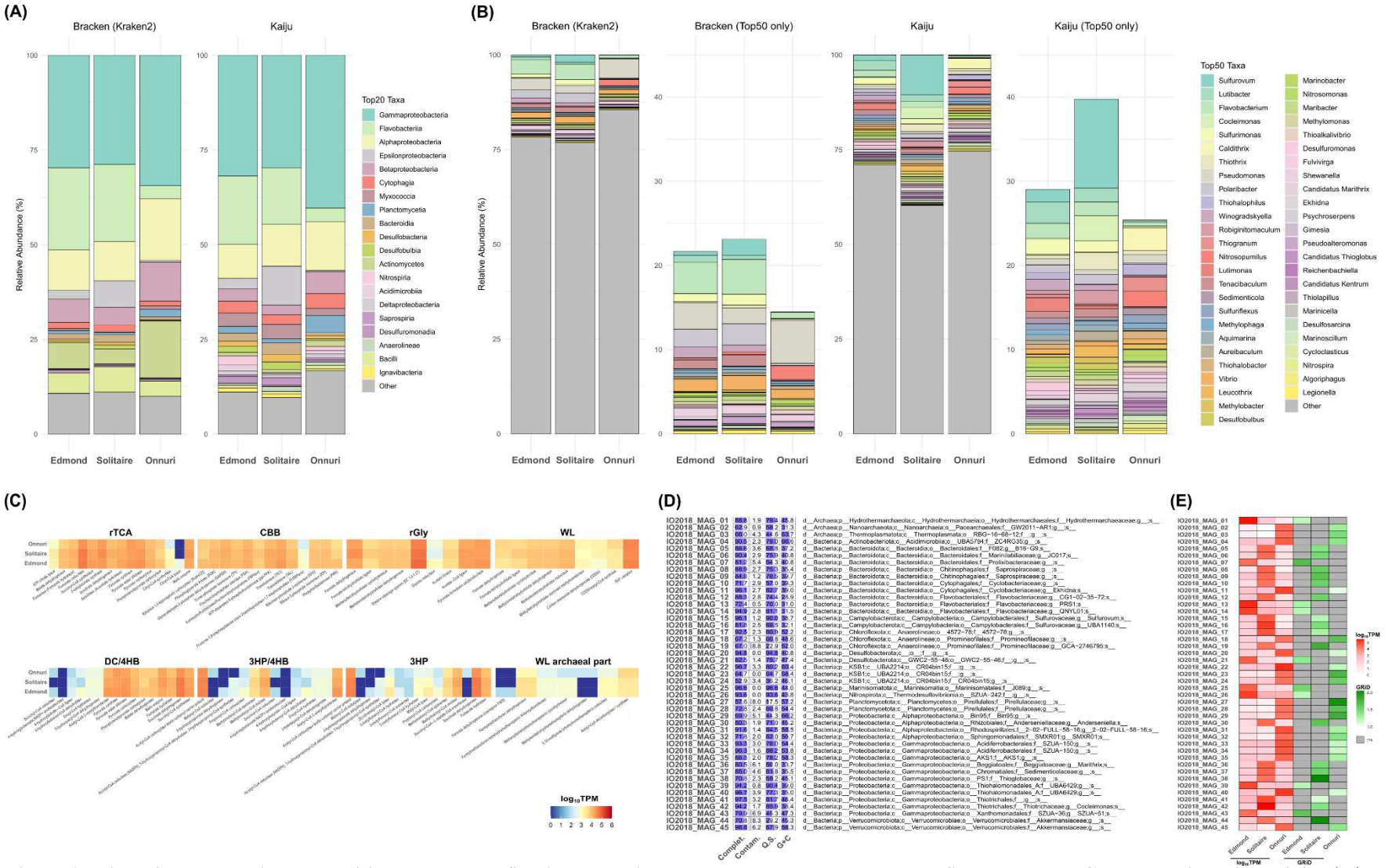


Figure 1. Microbial community composition and carbon fixation potential across three hydrothermal vent fields along the Central Indian Ridge. (A)Relative abundance of top 20 microbial taxa at the class level, classified by Kraken2-Bracken (left) and Kaiju (right). (B)Relative abundance of top 50 microbial taxa at the genus level excluding "Other", classified by Kraken2-Bracken (left) and Kaiju (right). (C)Heatmap of aggregated TPM values (log_{10}) for enzymes associated with seven carbon fixation pathways. (D)Quality metrics and GTDB-Tk-based taxonomic classification of recovered MAGs. (E)Heatmap of MAG relative abundance (log_{10}TPM) and replication rates (GRiD) across three vent fields.

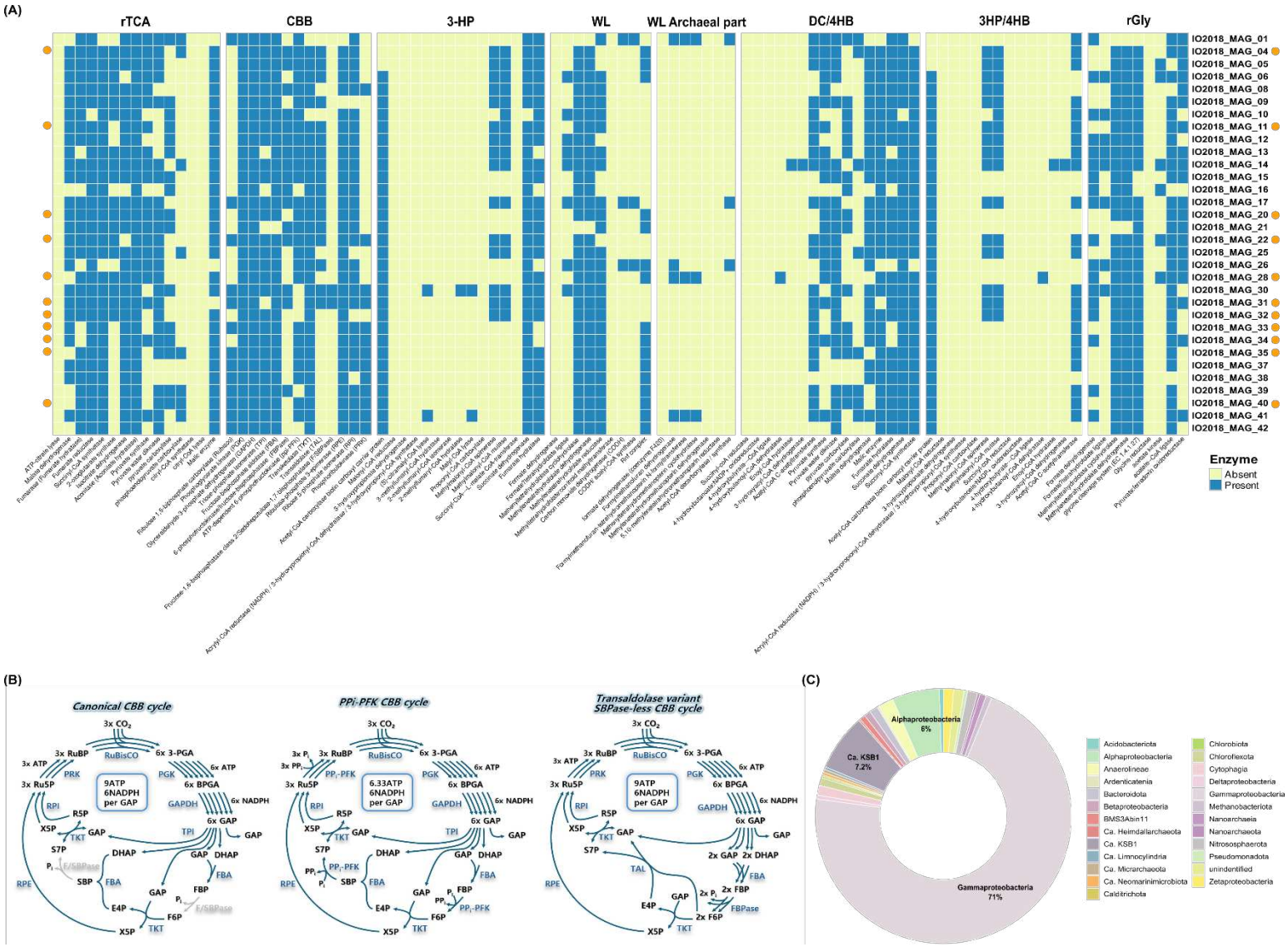


Figure 2. Carbon fixation potential of MAGs enriched in the OVF. (A)Presence or absence of enzymes associated with carbon fixation pathways across MAGs recovered in this study. Yellow circles indicate MAGs with high relative abundance in the OVF. (B Enzyme complement of IO2018_MAG_22 for canonical and non-canonical CBB cycle variants; gray labels indicate absent enzymes. (C)Donut chart showing the taxonomic composition of RuBisCO (RbcL) sequences detected in the OVF.

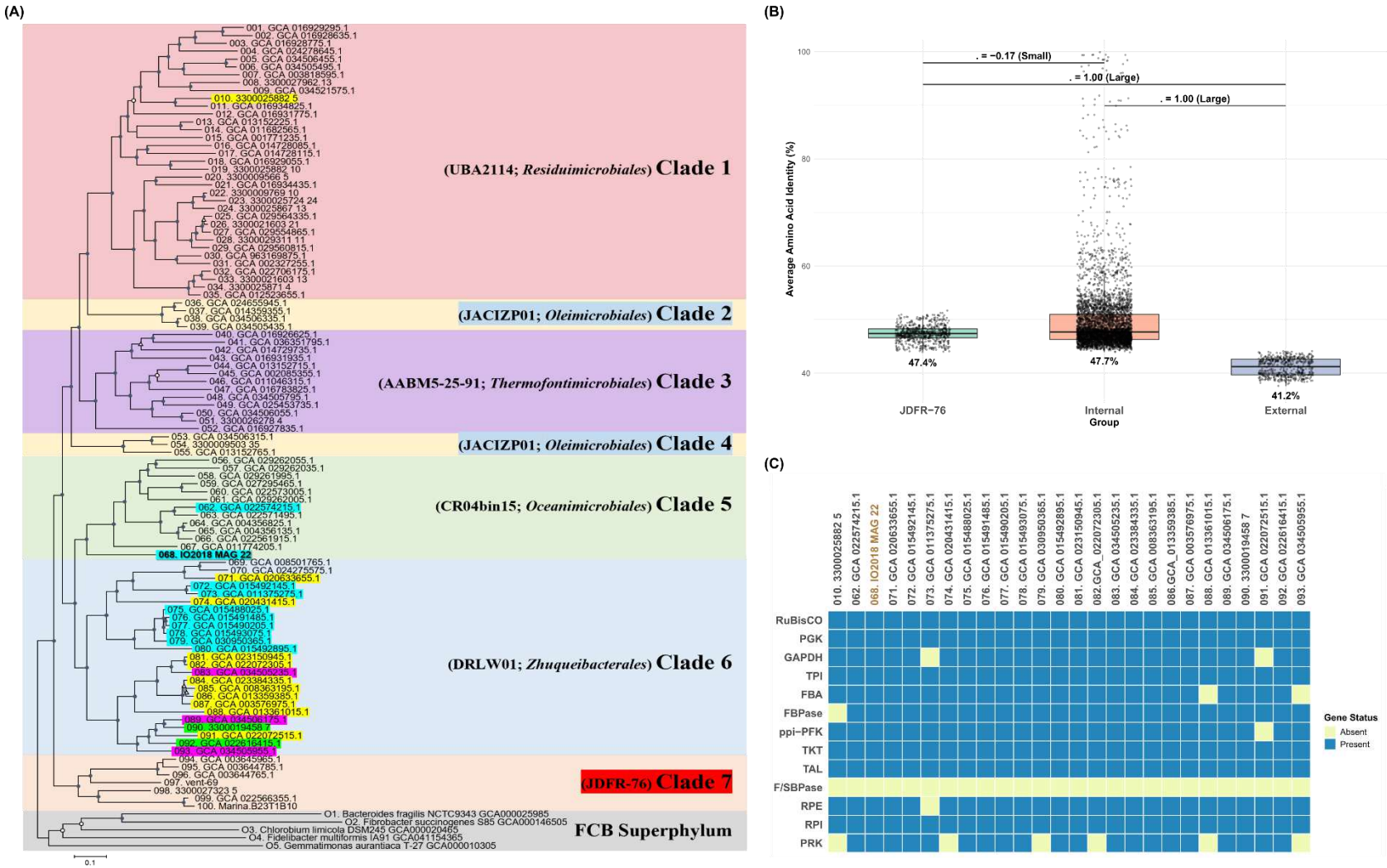


Figure 3. Phylogenomic analysis and carbon fixation potential of *Zhuqueibacterota*. (A)Maximum-likelihood phylogenomic tree of *Zhuqueibacterota* MAGs. Node support is indicated as follows: filled circles (●) for nodes with >90% support across all methods, (○) for nodes with 70–90% support, and triangles(△) for nodes where at least one method yielded <70% support. Colored backgrounds on MAG labels indicate the isolation source of RbcL-encoding MAGs: yellow, bioreactor; sky blue, deep-sea habitats; pink, terrestrial hot springs; green, cave wall deposits. (B)Pairwise AAI value distributions among three genome groups: JDFR-76 group (AAI between JDFR-76 members and other *Zhuqueibacterota* members), internal group (AAI among non-JDFR-76 *Zhuqueibacterota* members), and external group (AAI between all *Zhuqueibacterota* members including JDFR-76 and outgroup genomes). (C)Presence or absence of CBB cycle-associated enzymes across RbcL-encoding *Zhuqueibacterota* MAGs.

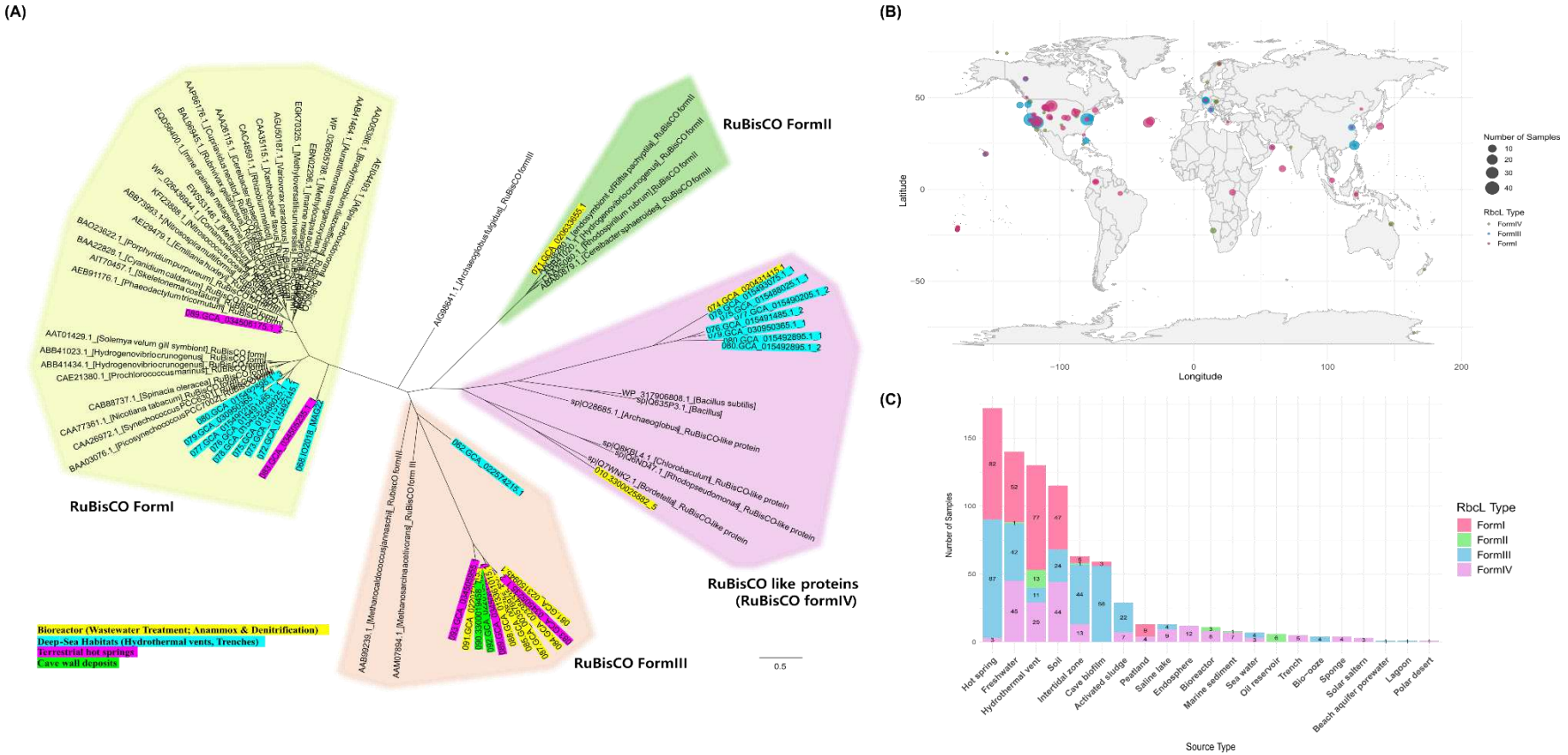


Figure 4. Phylogenetic analysis and global distribution of *Zhuqueibacterota*-derived RbcL sequences. (A)Maximum-likelihood phylogenetic tree of *Zhuqueibacterota*-derived and reference RbcL sequences. Colored backgrounds on MAG labels indicate *Zhuqueibacterota*-derived sequences, with colors representing isolation source type. (B)Global distribution map of *Zhuqueibacterota*-derived RbcL sequences identified by matching against metagenomic assemblies retrieved from the IMG/M database. (C)Distribution of RuBisCO forms among *Zhuqueibacterota* RbcL sequences grouped by isolation source type.

Acknowledgement

We thank all crew members and scientific participants of the IOR2018 cruise for their assistance during the expedition and sample collection.

Author Contributions

Mi-Jeong Park: Conceptualization; data curation; formal analysis; investigation; writing-original draft; writing-review and editing. **Yun Jae Kim:** Conceptualization; funding acquisition; resources; writing-review and editing. **Joungmin Lee:** Data curation; formal analysis; investigation; writing-original draft. **Jihyun Yu:** Data curation; formal analysis; investigation; writing-original draft. **Gyeong Hak Han:** Data curation; formal analysis; investigation; writing-original draft. **Jung-Hyun Lee:** Data curation; formal analysis; investigation; writing-original draft. **Kae Kyoung Kwon:** Conceptualization; funding acquisition; project administration; supervision; writing-review and editing.

Declarations

Ethics approval and consent to participate

Not applicable. This study did not involve human participants, human data, human tissue, or animal experimentation.

Consent for publication

Not applicable.

Availability of data and material

The assembled metagenomic contigs from the three vent fields dataset are publicly available under the following DOI: https://doi.org/10.5281/zenodo.22685631. The List of enzymes involved in carbon fixation pathways and their corresponding KEGG Orthology (KO) numbers and EC numbers dataset is provided in Supplementary Table 3. The Matching results of *Zhuqueibacterota*-derived RuBisCO (RbcL) sequences against the IMG/M database dataset are provided in Supplementary Table 9. The metagenome-assembled genomes (MAGs) recovered in this study are publicly available under the following DOI: https://doi.org/10.5281/zenodo.22684581. The Pairwise average amino acid identity (AAI) matrix of *Zhuqueibacterota* MAGs and outgroup genomes used for phylogenetic validation dataset is provided in Supplementary Table 8. The quality metrics, taxonomic classification, relative abundance, and replication rates (GRiD) of MAGs recovered from three hydrothermal vent fields dataset are provided in Supplementary Table 7. The shotgun metagenomic raw reads from the three hydrothermal vent fields dataset are available from the NCBI Sequence Read Archive under the following accession IDs: https://identifiers.org/ncbi/insdc.sra:SRR38145136, https://identifiers.org/ncbi/insdc.sra:SRR38145137, and https://identifiers.org/ncbi/insdc.sra:SRR38145138.

Competing interests

The authors declare that they have no conflict of interest.

Funding

This research was supported by the Ministry of Oceans and Fisheries, Republic of Korea (20170411, KS211514, KS211476) and the Korea Institute of Ocean Science and Technology (PE99922)

List of Figures

Figure 1. Microbial community composition and carbon fixation potential across three hydrothermal vent fields along the Central Indian Ridge.

Figure 2. Carbon fixation potential of MAGs enriched in the OVF.

Figure 3. Phylogenomic analysis and carbon fixation potential of *Zhuqueibacterota*.

Figure 4. Phylogenetic analysis and global distribution of *Zhuqueibacterota*-derived RbcL sequences.

List of Supplementary Materials

Supplementary Table 1. Sampling metadata for three hydrothermal vent fields along the Central Indian Ocean Ridge

Supplementary Table 2. Summary of quality trimming, read filtering, and taxonomic classification of metagenomic reads from three hydrothermal vent fields along the Central Indian Ridge.

Supplementary Table 3. List of enzymes involved in carbon fixation pathways and their corresponding KEGG Orthology (KO) numbers and EC numbers.

Supplementary Table 4. List of *Zhuqueibacterota* (formerly Ca. KSB1) metagenome-assembled genomes (MAGs) used in this study, including genome quality metrics and isolation source information.

Supplementary Table 5. Reference RuBisCO sequences representing each RuBisCO form and *Zhuqueibacterota*-derived RuBisCO sequences used for phylogenetic analysis.

Supplementary Table 6. Aggregated TPM values of carbon fixation pathway-associated enzymes across three hydrothermal vent fields along the Central Indian Ridge.

Supplementary Table 7. Quality metrics, taxonomic classification, relative abundance, and replication rates (GRiD) of MAGs recovered from three hydrothermal vent fields along the Central Indian Ridge.

Supplementary Table 8. Pairwise average amino acid identity (AAI) matrix of *Zhuqueibacterota* MAGs and outgroup genomes used for phylogenetic validation. Orange: AAI values among internal *Zhuqueibacterota* members (excluding JDFR-76); green: AAI values between JDFR-76 members and non-JDFR-76 *Zhuqueibacterota* members; blue: AAI values between all *Zhuqueibacterota* members and outgroup genomes.

Supplementary Table 9. Matching results of *Zhuqueibacterota*-derived RuBisCO (RbcL) sequences against the IMG/M database, including environmental metadata of matched metagenomes.

Supplementary Fig. 1. Sampling site map and representative photographs of three hydrothermal vent fields along the Central Indian Ridge.

548 **References**

549 1. Field, C.B., et al., *Primary production of the biosphere: integrating terrestrial and oceanic components.* science,
550 1998. **281**(5374): p. 237–240. https://10.1126/science.281.5374.237
551 2. Falkowski, P.G. and J.A. Raven, *Aquatic photosynthesis*. 2013: Princeton University Press.
552 https://doi.org/10.1515/9781400849727
553 3. Davies, T.W. and T. Smyth, *Redefining the photic zone: beyond the autotroph-centric view of light in the ocean.*
554 Communications Earth & Environment, 2025. **6**(1): p. 411. https://doi.org/10.1038/s43247-025-02374-2
555 4. Lutz, R.A. and M.J. Kennish, *Ecology of deep-sea hydrothermal vent communities: A review.* Reviews of
556 geophysics, 1993. **31**(3): p. 211–242. https://doi.org/10.1029/93RG01280
557 5. Jannasch, H.W. and C.O. Wirsen, *Chemosynthetic primary production at East Pacific sea floor spreading centers.*
558 Bioscience, 1979. **29**(10): p. 592–598. https://doi.org/10.2307/1307765
559 6. Jannasch, H.W. and M.J. Mottl, *Geomicrobiology of deep-sea hydrothermal vents.* Science, 1985. **229**(4715): p.
560 717–725. https://doi.org/10.1126/science.229.4715.717
561 7. Hou, J., et al., *Microbial succession during the transition from active to inactive stages of deep-sea hydrothermal*
562 *vent sulfide chimneys.* Microbiome, 2020. **8**(1): p. 102. https://doi.org/10.1186/s40168-020-00851-8
563 8. McNichol, J., et al., *Primary productivity below the seafloor at deep-sea hot springs.* Proceedings of the National
564 Academy of Sciences, 2018. **115**(26): p. 6756–6761. https://doi.org/10.1073/pnas.1804351115
565 9. Dick, G.J., *The microbiomes of deep-sea hydrothermal vents: distributed globally, shaped locally.* Nature
566 Reviews Microbiology, 2019. **17**(5): p. 271–283. https://doi.org/10.1038/s41579-019-0160-2
567 10. Meier, D.V., et al., *Niche partitioning of diverse sulfur-oxidizing bacteria at hydrothermal vents.* The ISME
568 journal, 2017. **11**(7): p. 1545–1558. https://doi.org/10.1038/ismej.2017.37
569 11. Cherkashov, G., *Seafloor massive sulfide deposits: Distribution and prospecting*, in *Deep-sea mining: Resource*
570 *potential, technical and environmental considerations*. 2017, Springer. p. 143–164. https://doi.org/10.1007/978-
571 3-319-52557-0_4
572 12. Kim, R.E., *The likely impact of the BBNJ Agreement on the architecture of ocean governance.* Marine Policy,
573 2024. **165**: p. 106190. https://doi.org/10.1016/j.marpol.2024.106190
574 13. Sievert, S.M. and C. Vetriani, *Chemoautotrophy at deep-sea vents: past, present, and future.* Oceanography,
575 2012. **25**(1): p. 218–233. https://doi.org/10.5670/oceanog.2012.21
576 14. Tao, C., et al., *Deep high-temperature hydrothermal circulation in a detachment faulting system on the ultra-*
577 *slow spreading ridge.* Nature communications, 2020. **11**(1): p. 1300. https://doi.org/10.1038/s41467-020-15062-
578 w
579 15. Perez, M., et al., *Structure and connectivity of hydrothermal vent communities along the mid-ocean ridges in the*
580 *West Indian Ocean: a review.* Frontiers in Marine Science, 2021. **8**: p. 744874.
581 https://doi.org/10.3389/fmars.2021.744874
582 16. Rudnicki, M.D. and C.R. German, *Temporal variability of the hydrothermal plume above the Kairei vent field,*
583 *25 S, Central Indian Ridge.* Geochemistry, Geophysics, Geosystems, 2002. **3**(2): p. XXX.
584 https://doi.org/10.1029/2001GC000240

17. Gallant, R. and K. Von Damm, *Geochemical controls on hydrothermal fluids from the Kairei and Edmond vent fields, 23–25 S, Central Indian Ridge.* Geochemistry, Geophysics, Geosystems, 2006. **7**(6): p. 1–24. https://doi.org/10.1029/2005GC001067
18. Nakamura, K., et al., *Discovery of new hydrothermal activity and chemosynthetic fauna on the Central Indian Ridge at 18–20 S.* PLoS one, 2012. **7**(3): p. e32965. https://doi.org/10.1371/journal.pone.0032965
19. Kim, J., et al., *Discovery of active hydrothermal vent fields along the Central Indian Ridge, 8–12 S.* Geochemistry, Geophysics, Geosystems, 2020. **21**(8): p. e2020GC009058. https://doi.org/10.1029/2020GC009058
20. Choi, K.-Y., et al., *Spatial variability of sediment geochemistry and meiofaunal communities in hydrothermal vent fields along the Central Indian ridge.* Marine Environmental Research, 2025: p. 107371. https://doi.org/10.1016/j.marenvres.2025.107371
21. Perner, M., et al., *Driving forces behind the biotope structures in two low-temperature hydrothermal venting sites on the southern Mid-Atlantic Ridge.* Environmental Microbiology Reports, 2011. **3**(6): p. 727–737. https://doi.org/10.1111/j.1758-2229.2011.00291.x
22. Olins, H., et al., *Assessing the influence of physical, geochemical and biological factors on anaerobic microbial primary productivity within hydrothermal vent chimneys.* Geobiology, 2013. **11**(3): p. 279–293. https://doi.org/10.1111/gbi.12034
23. Olins, H., et al., *Co-registered Geochemistry and Metatranscriptomics Reveal Unexpected Distributions of Microbial Activity within a Hydrothermal Vent Field, Front. Microbiol., 8, 1042*. 2017. https://doi.org/10.3389/fmicb.2017.01042
24. Lim, D., et al., *Characterization of geochemistry in hydrothermal sediments from the newly discovered onnuri vent field in the middle region of the Central Indian Ridge.* Frontiers in Marine Science, 2022. **9**: p. 810949. https://doi.org/10.3389/fmars.2022.810949
25. Van Dover, C.L., et al., *Biogeography and ecological setting of Indian Ocean hydrothermal vents.* Science, 2001. **294**(5543): p. 818–823. https://doi.org/10.3389/fmars.2022.1067912
26. Kim, M., J.-H. Kang, and D. Kim, *Holoplanktonic and meroplanktonic larvae in the surface waters of the Onnuri Vent Field in the Central Indian Ridge.* Journal of Marine Science and Engineering, 2022. **10**(2): p. 158. https://doi.org/10.3390/jmse10020158
27. Ryu, T., et al., *First transcriptome assembly of a newly discovered vent mussel, Gigantidas vrijenhoeki, at Onnuri Vent Field on the northern Central Indian Ridge.* Marine Genomics, 2021. **57**: p. 100819. https://doi.org/10.1016/j.margen.2020.100819
28. Jang, S.-J., et al., *Connectivity and divergence of symbiotic bacteria of deep-sea hydrothermal vent mussels in relation to the structure and dynamics of mid-ocean ridges.* Frontiers in Marine Science, 2022. **9**: p. 845965. https://doi.org/10.3389/fmars.2022.845965
29. Jang, S.-J., et al., *A newly discovered Gigantidas bivalve mussel from the Onnuri Vent Field in the northern Central Indian Ridge.* Deep Sea Research Part I: Oceanographic Research Papers, 2020. **161**: p. 103299. https://doi.org/10.1016/j.dsr.2020.103299
30. Mao, Q., et al., *Genetic Structure in a Trans-Oceanic Hot Vent Mussel Reveals Four Metapopulations With*

Implications for Conservation. Journal of Biogeography, 2025. **52**(10): p. e70017. https://doi.org/10.1111/jbi.70017

31. Jang, S.-J., et al., *Geographical subdivision of Alviniconcha snail populations in the Indian Ocean hydrothermal vent regions.* Frontiers in Marine Science, 2023. **10**: p. 1139190. https://doi.org/10.3389/fmars.2023.1139190
32. Choi, H., O.-H. Yu, and S.-i. Eyun, *Evolutionary insights into adaptation of hemocyanins from deep-sea hydrothermal vent shrimps.* Marine Pollution Bulletin, 2025. **215**: p. 117872. https://doi.org/10.1016/j.marpolbul.2025.117872
33. Cho, B., et al., *Unique characteristics of the exoskeleton of bythograeid crab, Austinograea rodriguezensis in the indian ocean hydrothermal vent (onnuri vent field).* Integrative and Comparative Biology, 2020. **60**(1): p. 24–32. https://doi.org/10.1093/icb/icz150
34. Cho, B., D. Kim, and T. Kim, *Exceptional properties of hyper-resistant armor of a hydrothermal vent crab.* Scientific Reports, 2022. **12**(1): p. 11816. https://doi.org/10.1038/s41598-022-15982-1
35. Suh, Y.J., et al., *Trophic diversity of chemosymbiont hosts in deep-sea hydrothermal vents using amino acid nitrogen isotopes.* Frontiers in Marine Science, 2023. **10**: p. 1204992. https://doi.org/10.3389/fmars.2023.1204992
36. Hwang, H.-s., et al., *New record of hydrothermal vent squat lobster (Munidopsis lauensis) provides evidence of a dispersal corridor between the Pacific and Indian oceans.* Journal of Marine Science and Engineering, 2022. **10**(3): p. 400. https://doi.org/10.3390/jmse10030400
37. Kim, S.L., et al., *A new Branchipolynoe (Aphroditiformia: Polynoidae) scale worm from the Onnuri Deep-sea hydrothermal vent field, northern Central Indian Ridge.* Zoological Studies, 2022. **61**: p. e21. https://doi.org/10.6620/ZS.2022.61-21
38. Lee, W.-K. and S.-J. Kim, *Distribution extension of a vent scale worm Branchinotoglumabipapillata (Polychaeta, Polynoidae) in the Indian Ocean.* ZooKeys, 2024. **1215**: p. 139. https://doi.org/10.3897/zookeys.1215.129623
39. Kim, J.G. and J. Lee, *A new species of the genus Smacigastes Ivanenko & Defaye, 2004 (Tegastidae, Harpacticoida, Copepoda) from the Onnuri Vent Field in the Indian Ocean.* Zoosystematics and Evolution, 2020. **96**(2): p. 699–714. https://doi.org/10.3897/zse.96.54507
40. Ivanenko, V.N., et al., *Description of Barathricolathermophilus, a new species from a deep-sea hydrothermal vent field in the Indian Ocean with redescription of the Barathricola type species (Crustacea, Copepoda, Cyclopoida).* ZooKeys, 2019. **865**: p. 103. https://doi.org/10.3897/zookeys.865.35827
41. Choi, J.M., D.S. Kim, and Y.-O. Kim, *Morphology and phylogenetic position of two novel Dysteria species (Ciliophora: Cyrtophoria) from deep-sea hydrothermal vents on the Central Indian Ridge, Indian Ocean.* Systematics and Biodiversity, 2025. **23**(1): p. 2435839. https://doi.org/10.1080/14772000.2024.2435839
42. Kim, M., et al., *Characterization of the mitochondrial genome, ecological distribution, and morphological features of the marine gastropod mollusc Lophocochlias parvissimus (Gastropoda, Tornidae).* Journal of Marine Science and Engineering, 2023. **11**(12): p. 2307. https://doi.org/10.3390/jmse11122307
43. Kang, T. and D. Kim, *Meiofauna and nematode community composition in a hydrothermal vent and deep-sea*

sediments in the Central Indian Ridge. Marine pollution bulletin, 2021. **170**: p. 112616. https://doi.org/10.1016/j.marpolbul.2021.112616

44. Suh, Y.J., et al., *Carbon sources and trophic interactions of vent fauna in the Onnuri Vent Field, Indian Ocean, inferred from stable isotopes.* Deep Sea Research Part I: Oceanographic Research Papers, 2022. **182**: p. 103683. https://doi.org/10.1016/j.dsr.2021.103683
45. Namirimu, T., et al., *Microbial diversity of deep-sea sediments from three newly discovered hydrothermal vent fields in the central Indian ridge.* Ocean Science Journal, 2023. **58**(2): p. 11. https://doi.org/10.1007/s12601-023-00106-1
46. Namirimu, T., et al., *Microbial community structure and functional potential of Deep-Sea sediments on low activity hydrothermal area in the central Indian ridge.* Frontiers in Marine Science, 2022. **9**: p. 784807. https://doi.org/10.3389/fmars.2022.784807
47. Tanner, M.A., et al., *Complex microbial communities inhabiting sulfide-rich black mud from marine coastal environments.* Biotechnology et alia, 2000. **8**: p. 1–16.
48. Baker, B.J., et al., *Genomic resolution of linkages in carbon, nitrogen, and sulfur cycling among widespread estuary sediment bacteria.* Microbiome, 2015. **3**(1): p. 14. https://doi.org/10.1186/s40168-015-0077-6
49. Dombrowski, N., et al., *Genomic insights into potential interdependencies in microbial hydrocarbon and nutrient cycling in hydrothermal sediments.* Microbiome, 2017. **5**(1): p. 106. https://doi.org/10.1186/s40168-017-0322-2
50. Dalcin Martins, P., et al., *Wetland sediments host diverse microbial taxa capable of cycling alcohols.* Applied and Environmental Microbiology, 2019. **85**(12): p. e00189–19. https://doi.org/10.1128/AEM.00189-19
51. Li, H., et al., *CPJSdraw: analysis and visualization of junction sites of chloroplast genomes.* PeerJ, 2023. **11**: p. e15326. https://doi.org/10.7717/peerj.15326
52. Lian, Z.H., et al., *Metagenomic analysis sheds light on the mixotrophic lifestyle of bacterial phylum Zhuqueibacterota.* Imeta, 2024. **3**(6): p. e249. https://doi.org/10.1002/imt2.249
53. Jiang, H., et al., *Skewer: a fast and accurate adapter trimmer for next-generation sequencing paired-end reads.* BMC bioinformatics, 2014. **15**(1): p. 182. https://doi.org/10.1186/1471-2105-15-182
54. Bushnell, B., *BBMap: a fast, accurate, splice-aware aligner.* 2014.
55. Nurk, S., et al., *metaSPAdes: a new versatile metagenomic assembler.* Genome research, 2017. **27**(5): p. 824–834. https://doi.org/10.1101/gr.213959.116
56. Wood, D.E., J. Lu, and B. Langmead, *Improved metagenomic analysis with Kraken 2.* Genome biology, 2019. **20**(1): p. 257. https://doi.org/10.1186/s13059-019-1891-0
57. Lu, J., et al., *Bracken: estimating species abundance in metagenomics data.* PeerJ Computer Science, 2017. **3**: p. e104. https://doi.org/10.7717/peerj-cs.104
58. Menzel, P., K.L. Ng, and A. Krogh, *Fast and sensitive taxonomic classification for metagenomics with Kaiju.* Nature communications, 2016. **7**(1): p. 11257. https://doi.org/10.1038/ncomms11257
59. Hyatt, D., et al., *Prodigal: prokaryotic gene recognition and translation initiation site identification.* BMC bioinformatics, 2010. **11**(1): p. 119. https://doi.org/10.1186/1471-2105-11-119
60. Cantalapiedra, C.P., et al., *eggNOG-mapper v2: functional annotation, orthology assignments, and domain*

prediction at the metagenomic scale. Molecular biology and evolution, 2021. **38**(12): p. 5825–5829. https://doi.org/10.1093/molbev/msab293

61. Huerta-Cepas, J., et al., *eggNOG 5.0: a hierarchical, functionally and phylogenetically annotated orthology resource based on 5090 organisms and 2502 viruses.* Nucleic acids research, 2019. **47**(D1): p. D309–D314. https://doi.org/10.1093/nar/gky1085
62. Li, H. and R. Durbin, *Fast and accurate short read alignment with Burrows–Wheeler transform.* bioinformatics, 2009. **25**(14): p. 1754–1760. https://doi.org/10.1093/bioinformatics/btp324
63. Li, H., et al., *The sequence alignment/map format and SAMtools.* bioinformatics, 2009. **25**(16): p. 2078–2079. https://doi.org/10.1093/bioinformatics/btp352
64. Greco, C., et al., *Genome-resolved metagenomics reveals diverse taxa and metabolic complexity in Antarctic lake microbial structures.* Environmental Microbiology, 2024. **26**(6): p. e16663. https://doi.org/10.1111/1462-2920.16663
65. Alneberg, J., et al., *Binning metagenomic contigs by coverage and composition.* Nature methods, 2014. **11**(11): p. 1144–1146. https://doi.org/10.1038/nmeth.3103
66. Kang, D.D., et al., *MetaBAT 2: an adaptive binning algorithm for robust and efficient genome reconstruction from metagenome assemblies.* PeerJ, 2019. **7**: p. e7359. https://doi.org/10.7717/peerj.7359
67. Wu, Y.-W., B.A. Simmons, and S.W. Singer, *MaxBin 2.0: an automated binning algorithm to recover genomes from multiple metagenomic datasets.* Bioinformatics, 2016. **32**(4): p. 605–607. https://doi.org/10.1093/bioinformatics/btv638
68. Sieber, C.M., et al., *Recovery of genomes from metagenomes via a dereplication, aggregation and scoring strategy.* Nature microbiology, 2018. **3**(7): p. 836–843. https://doi.org/10.1038/s41564-018-0171-1
69. Parks, D.H., et al., *Recovery of nearly 8,000 metagenome-assembled genomes substantially expands the tree of life.* Nature microbiology, 2017. **2**(11): p. 1533–1542. https://doi.org/10.1038/s41564-017-0083-5
70. Parks, D.H., et al., *CheckM: assessing the quality of microbial genomes recovered from isolates, single cells, and metagenomes.* Genome research, 2015. **25**(7): p. 1043–1055. https://doi.org/10.1101/gr.186072.114
71. Bowers, R.M., et al., *Minimum information about a single amplified genome (MISAG) and a metagenome-assembled genome (MIMAG) of bacteria and archaea.* Nature biotechnology, 2017. **35**(8): p. 725–731. https://doi.org/10.1038/nbt0718-660a
72. Chaumeil, P.-A., et al., *GTDB-Tk: a toolkit to classify genomes with the Genome Taxonomy Database*. 2020, Oxford University Press. https://doi.org/10.1093/bioinformatics/btz848
73. Emiola, A. and J. Oh, *High throughput in situ metagenomic measurement of bacterial replication at ultra-low sequencing coverage.* Nature communications, 2018. **9**(1): p. 4956. https://doi.org/10.1038/s41467-018-07240-8
74. Shaffer, M., et al., *DRAM for distilling microbial metabolism to automate the curation of microbiome function.* Nucleic acids research, 2020. **48**(16): p. 8883–8900. https://doi.org/10.1093/nar/gkaa621
75. Aramaki, T., et al., *KofamKOALA: KEGG Ortholog assignment based on profile HMM and adaptive score threshold.* Bioinformatics, 2020. **36**(7): p. 2251–2252. https://doi.org/10.1093/bioinformatics/btz859

76. Wang, Y., et al., *A crowdsourcing open platform for literature curation in UniProt.* PLoS biology, 2021. **19**(12): p. e3001464. https://doi.org/10.1371/journal.pbio.3001464
77. Paysan-Lafosse, T., et al., *The Pfam protein families database: embracing AI/ML.* Nucleic acids research, 2025. **53**(D1): p. D523–D534. https://doi.org/10.1093/nar/gkae1276
78. Yin, Y., et al., *dbCAN: a web resource for automated carbohydrate-active enzyme annotation.* Nucleic acids research, 2012. **40**(W1): p. W445–W451. https://doi.org/10.1093/nar/gks479
79. Trgovec-Greif, L., et al., *VOGDB—database of virus orthologous groups.* Viruses, 2024. **16**(8): p. 1191. https://doi.org/10.3390/v16081191
80. Olm, M.R., et al., *dRep: a tool for fast and accurate genomic comparisons that enables improved genome recovery from metagenomes through de-replication.* The ISME journal, 2017. **11**(12): p. 2864–2868. https://doi.org/10.1038/ismej.2017.126
81. Katoh, K. and D.M. Standley, *MAFFT multiple sequence alignment software version 7: improvements in performance and usability.* Molecular biology and evolution, 2013. **30**(4): p. 772–780. https://doi.org/10.1093/molbev/mst010
82. Minh, B.Q., et al., *IQ-TREE 2: new models and efficient methods for phylogenetic inference in the genomic era.* Molecular biology and evolution, 2020. **37**(5): p. 1530–1534. https://doi.org/10.1093/molbev/msaa131
83. Kim, D., S. Park, and J. Chun, *Introducing EzAAI: a pipeline for high throughput calculations of prokaryotic average amino acid identity.* Journal of Microbiology, 2021. **59**(5): p. 476–480. https://doi.org/10.1007/s12275-023-00075-z
84. Romano, J., et al. *Exploring methods for evaluating group differences on the NSSE and other surveys: Are the t-test and Cohen'sd indices the most appropriate choices*. in *annual meeting of the Southern Association for Institutional Research*. 2006. Citeseer.
85. Kanehisa, M., Y. Sato, and K. Morishima, *BlastKOALA and GhostKOALA: KEGG tools for functional characterization of genome and metagenome sequences.* Journal of molecular biology, 2016. **428**(4): p. 726–731. https://doi.org/10.1016/j.jmb.2015.11.006
86. Capella-Gutiérrez, S., J.M. Silla-Martínez, and T. Gabaldón, *trimAl: a tool for automated alignment trimming in large-scale phylogenetic analyses.* Bioinformatics, 2009. **25**(15): p. 1972–1973. https://doi.org/10.1093/bioinformatics/btp348
87. Chen, I.-M.A., et al., *The IMG/M data management and analysis system v. 7: content updates and new features.* Nucleic acids research, 2023. **51**(D1): p. D723–D732. https://doi.org/10.1093/nar/gkac976
88. Buchfink, B., C. Xie, and D.H. Huson, *Fast and sensitive protein alignment using DIAMOND.* Nature methods, 2015. **12**(1): p. 59–60. https://doi.org/10.1038/nmeth.3176
89. Wissuwa, J., et al., *Complete genome sequence of Lutibacter profundi LP1T isolated from an Arctic deep-sea hydrothermal vent system.* Standards in Genomic Sciences, 2017. **12**(1): p. 5. https://doi.org/10.1186/s40793-016-0219-x
90. Wasmund, K., et al., *Genomic insights into diverse bacterial taxa that degrade extracellular DNA in marine sediments.* Nature Microbiology, 2021. **6**(7): p. 885–898. https://doi.org/10.1038/s41564-021-00917-9

91. Yadav, S., et al., *Organic matter degradation in the deep, sulfidic waters of the Black Sea: insights into the ecophysiology of novel anaerobic bacteria.* Microbiome, 2024. **12**(1): p. 98. https://doi.org/10.1186/s40168-024-01816-x
92. Song, W., et al., *Distinct patterns of microbial association across deep-sea corals from the Western Pacific Magellan Seamounts.* Microbiology Spectrum, 2025. **14**(1): p. e02093–25. https://doi.org/10.1128/spectrum.02093-25
93. Könneke, M., et al., *Isolation of an autotrophic ammonia-oxidizing marine archaeon.* Nature, 2005. **437**(7058): p. 543–546. https://doi.org/10.1038/nature03911
94. Koch, H., et al., *Expanded metabolic versatility of ubiquitous nitrite-oxidizing bacteria from the genus Nitrospira.* Proceedings of the national academy of sciences, 2015. **112**(36): p. 11371–11376. https://doi.org/10.1073/pnas.1506533112
95. Walker, C., et al., *Nitrosopumilus maritimus genome reveals unique mechanisms for nitrification and autotrophy in globally distributed marine crenarchaea.* Proceedings of the National Academy of Sciences, 2010. **107**(19): p. 8818–8823. https://doi.org/10.1073/pnas.0913533107
96. Zhao, Z., et al., *Discovery of Candidatus Nitrosomaritimum as a new genus of ammonia-oxidizing archaea widespread in anoxic saltmarsh intertidal aquifers.* Environmental Science & Technology, 2024. **58**(36): p. 16040–16054. https://doi.org/10.1021/acs.est.4c02321
97. Han, Y. and M. Perner, *The globally widespread genus Sulfurimonas: versatile energy metabolisms and adaptations to redox clines.* Frontiers in microbiology, 2015. **6**: p. 989. https://doi.org/10.3389/fmicb.2015.00989
98. Sun, Q.-L., et al., *High-throughput sequencing reveals a potentially novel Sulfurovum species dominating the microbial communities of the seawater–sediment interface of a deep-sea cold seep in South China sea.* Microorganisms, 2020. **8**(5): p. 687. https://doi.org/10.3390/microorganisms8050687
99. Wang, L., et al., *Diversity of total bacterial communities and chemoautotrophic populations in sulfur-rich sediments of shallow-water hydrothermal vents off Kueishan Island, Taiwan.* Microbial ecology, 2017. **73**(3): p. 571–582. https://doi.org/10.1007/s00248-016-0898-2
100. Biegel, E., et al., *Biochemistry, evolution and physiological function of the Rnf complex, a novel ion-motive electron transport complex in prokaryotes.* Cellular and molecular life sciences, 2011. **68**(4): p. 613–634. https://doi.org/10.1007/s00018-010-0555-8
101. Hudson, E.P. *The Calvin Benson cycle in bacteria: new insights from systems biology*. in *Seminars in Cell & Developmental Biology*. 2024. Elsevier. https://doi.org/10.1016/j.semcdb.2023.03.007